



Contents lists available at ScienceDirect

Bioorganic & Medicinal Chemistry

journal homepage: www.elsevier.com/locate/bmc

Rational design of inhibitors of the bacterial cell wall synthetic enzyme GlmU using virtual screening and lead-hopping



Peter Doig^{a,*}, P. Ann Boriack-Sjodin^a, Jacques Dumas^b, Jun Hu^a, Kenji Itoh^c, Kenneth Johnson^b, Steven Kazmirski^a, Tomohiko Kinoshita^c, Satoru Kuroda^c, Tomo-o Sato^c, Kaori Sugimoto^c, Katsumi Tohyama^c, Hiroshi Aoi^c, Kazusa Wakamatsu^c, Hongming Wang^b

^a Discovery Sciences, AstraZeneca R&D Boston, 35 Gatehouse Drive, Waltham, MA 02451, United States

^b Infection Innovative Medicines, AstraZeneca R&D Boston, Waltham, MA 02451, United States

^c Wakunaga Pharmaceutical Co. Ltd, Akitakata City, Hiroshima 739-1195, Japan

ARTICLE INFO

Article history:

Received 1 November 2013

Revised 6 August 2014

Accepted 18 August 2014

Available online 16 September 2014

Keywords:

GlmU

Aminoquinazoline

Cell wall biosynthesis

N-Acetylglucosamine-1-phosphate

Uridyltransferase

Virtual screening

ABSTRACT

An aminoquinazoline series targeting the essential bacterial enzyme GlmU (uridylyltransferase) were previously reported (*Biochem. J.* **2012**, 446, 405). In this study, we further explored SAR through a combination of traditional medicinal chemistry and structure-based drug design, resulting in a novel scaffold (benzamide) with selectivity against protein kinases. Virtual screening identified fragments that could be fused into the core scaffold, exploiting additional binding interactions and thus improving potency. These efforts resulted in a hybrid compound with target potency increased by a 1000-fold, while maintaining selectivity against selected protein kinases and an improved level of solubility and protein binding. Despite these significant improvements no significant antibacterial activity was yet observed within this class.

© 2014 Elsevier Ltd. All rights reserved.

1. Introduction

Bacterial resistance to marketed antibiotics is a growing threat to their efficacy and continued use in the clinic.¹ This is particularly true for Gram-negative bacteria, for which effective options for the treatment of new resistant forms (e.g., New Delhi metallo-beta-lactamase 1) continue to diminish. In the search for the next generation of antibiotics, circumventing existing resistance that resides within the clinic has become the focus. One such approach exploits novel targets for which mechanism-based resistance is absent in the bacterial pools found in hospitals and other care centers.

GlmU is a bifunctional enzyme that converts D-glucosamine-1-phosphate (GlcN-1-P) into uridyldiphosphate-N-acetylglucosamine (UDP-GlcNAc), an essential precursor in both lipopolysaccharide and peptidoglycan synthesis in bacteria. The enzyme catalyzes two separate reactions in two distinctly separate structural domains. The first reaction transfers an acetyl group from acetyl-CoA to glucosamine-1-phosphate producing N-acetylglucosamine-1-phosphate (GlcNAc-1-P) and CoA.² This reaction occurs in the carboxy-terminal end of the polypeptide. The second reaction

transfers uridylyl monophosphate from UTP to form UDP-GlcNAc and a pyrophosphate ion (PP_i) and takes place entirely within the N-terminal domain. Inhibitors of this enzyme would be expected to have a dual mode of action in Gram-negative bacteria, preventing both peptidoglycan and lipopolysaccharide synthesis, making it an excellent target for drug discovery. In addition, absence of an equivalent enzyme in humans makes GlmU especially attractive as a target for antibacterial drug design.³

Recent efforts have been fruitful in finding small molecule inhibitors to both the C-terminal acetyltransferase domain^{4,5} and the N-terminal uridylyltransferase domain.^{6,7} The sulfonamide acetyltransferase inhibitors described by Buurman et al.⁴ have been used to validate GlmU as a productive antibacterial target. Their studies demonstrated that a potent inhibitor of GlmU function has antibacterial properties consistent with disruption of peptidoglycan and fatty acid biosyntheses.⁴ Further, mutants resistant to the action of the sulfonamides were generated and the mutations responsible for the resistance phenotype shown to reside in the GlmU acetyltransferase domain.

The 4-anilino-quinazolines, exemplified by compound **1**, were recently identified by high-throughput screening (HTS) and database mining.⁷ These analogs provide a starting point for the design of potent GlmU inhibitors. This series inhibits Gram-negative

* Corresponding author. Tel.: +1 781 839 5434; fax: +1 781 839 4570.

E-mail address: Peter.Doig@astrazeneca.com (P. Doig).

isozymes, but have poor activity against Gram-positive isozymes. This finding and a subsequent analysis of the binding mode from crystallographic studies suggest the potential for further optimization as Gram-negative specific agents. Compound **1** exhibits an unexpected binding mode (Fig. 1). Despite being competitive with UTP, the quinazoline ring binds into the ribose pocket of GlmU rather than directly into the uracil pocket, via a single hydrogen bond between the 7-position hydroxyl and the backbone of Ala13 (also formed by the 2-oxygen in the uracil ring of UTP). The lead does not exploit key hydrogen bonding interactions of the uracil pocket, notably with Gln76, nor does it extend into the GlcNAc binding pocket (Fig. 1). In addition, significant Aurora kinase B inhibitory activity is observed in biochemical assays. We expected that by maintaining and optimizing the two ends of this lead series, improved potency and selectivity could be achieved.

Virtual screening (VS) based on either pharmacophore models or docking is well precedent as an approach to finding and improving inhibitor series.⁸ The success of this approach is greatly aided by an understanding of the binding mode and ligand binding constraints. Using VS to grow existing inhibitors towards unfilled binding pockets has been employed to improve potency, usually by linking known fragments into a large, more potent molecule. More rarely was it employed to identify fragments to further drive potency.

In this study, a combination of traditional medicinal chemistry and virtual screening resulted in a hybrid compound with ~1000-fold increased potency against GlmU, with selectivity towards selected protein kinases.

2. Results

2.1. Structure–activity relationships: Progress towards GlcNAc and uracil pockets and kinase selectivity

The first synthetic chemistry efforts were to explore the uracil and GlcNAc (sugar) pockets of GlmU to improve the potency of the initial hit, while addressing the kinase selectivity of the series. A close examination of the compound **1** binding mode (Fig. 1) suggested that substitution at the C2 position of the quinazoline ring of compound **1** could result in interactions with the GlcNAc pocket.

In addition, it is well known in the literature that substitution at this position is not tolerated for binding into protein kinases, due to a steric clash with the backbone of the hinge region.⁹

The result of C2 exploration is outlined in Table 1. Results of simple substitution at C2 such as methyl (**5a**), amino (**10**), and chloro (**11**) were encouraging, as GlmU inhibitory activities were maintained in the low micromolar range. This led to the belief that key hydrogen bonds are largely maintained with the C2 substitution. Additionally, Aurora kinase B selectivity was greatly improved as both **5a** and **10** showed >30 μ M IC₅₀ (Table 2). Although early prototypes such as **5b** and **5c** did not extend all the way to the sugar pocket of the active site and made few if any interactions with the enzyme (Fig. 2A), these compounds highlighted the potential of C2 as a vector towards this region of the enzyme, and maintained a high level of selectivity against kinases tested. The most extended analogs **12a** and **12b** were designed to extend deeper in the pocket. Potencies in the biochemical assays were mostly unchanged against *Escherichia coli*, but sometimes improved against *Haemophilus influenzae*. However, all analogs failed to make productive hydrogen bond contacts with residues in the GlcNAc pocket. Additionally, low aqueous solubilities and high plasma protein binding remained, although the potential for higher solubility was observed with **12b**. With these results, further exploration of the GlcNAc pocket was abandoned.

Modeling data suggested that the hydroxyl group of the quinazoline at C7 could be used as a vector towards the uracil pocket, and several analogs were prepared to test this hypothesis (**7a**, **7b**, and **7c**). Of these, **7b** showed the most promise with an improved aqueous solubility and balanced *E. coli*/*H. influenzae* GlmU activity in the micromolar range (Table 1). The crystal structure showed that the potency lost due to the lack of H-bond with Ala13 is partially offset by two new hydrogen bonds formed with Gln76 and Gln79 in the uracil pocket (Fig. 2B).

Based on the modest results obtained from the exploitation of the C2 position of the quinazoline scaffold, scaffold hopping was pursued as an alternative approach to decrease kinase activity. As the nitrogen at position one of the scaffolds does not interact with residues in the N-terminal domain of GlmU, but is key binding element for protein kinases, the decision was made to remove it from the core structure. The 2-aminobenzamide **16b**

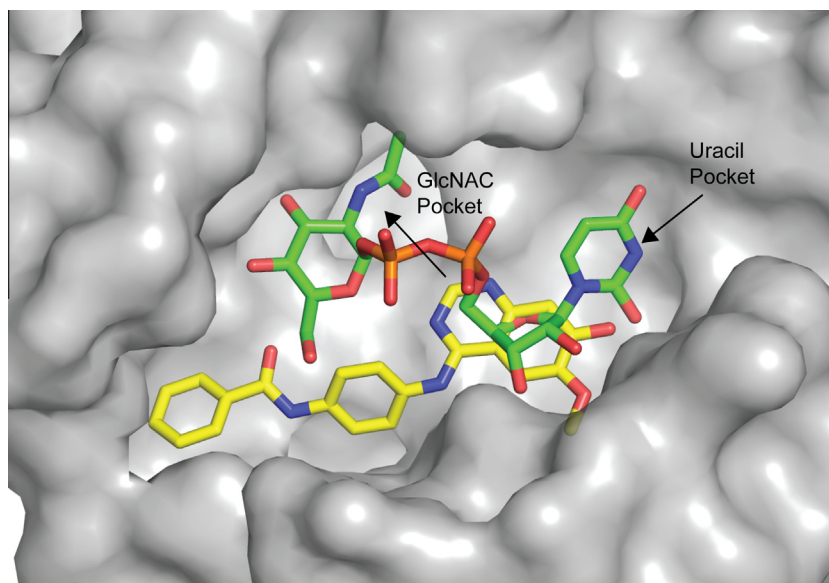
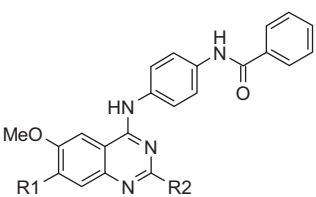


Figure 1. Quinazoline lead structure compound **1** (light grey/green⁷; PDB code 4E1K) superimposed with the structure of the UDP-GlcNAc product in *H. influenzae* GlmU (dark grey²³; PDB code 2V0I). The uracil and GlcNAc binding areas and the vectors from the lead compound that target those areas are indicated.

Table 1



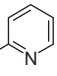
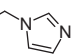
Compound	R1	R2	IC ₅₀ (μM)		Solubility			Serum binding (%)
			<i>E. coli</i>	<i>H. influenzae</i>	pH 3.5	pH 7.0	pH 8.0	
1	OH	H	1.3 ± 0.3	0.26 ± 0.04	—	—	—	—
5a	OH	CH ₃	2.2 ± 0.8	0.39 ± 0.11	20	46	169	90.3
5b	OH	2-Pyridyl	2.7 ± 0.8	1.5 ± 1.2	0.2	1.5	6.3	>99
5c	OH	–Bn	4.8±	1.8±	0.5	0.6	2.5	>99
7a	HOCH ₂ CH ₂ O*	H	35±	19±	—	—	—	—
7b	HOCH ₂ CH ₂ O*	H	6.7 ± 0.3	3.2 ± 1.3	14	169	178	>99
7c	H ₂ NCH ₂ CH ₂ O*	H	>22	>22	—	—	—	—
10	OH	NH ₂	10.5 ± 5.1	1.7 ± 0.01	12	14	39	97.7
11	OH	Cl	0.37 ± 0.11	0.65 ± 0.15	2.2	4.9	75	97.9
12a	OH		0.65 ± 0.05	0.38 ± .01	63	1.1	4.7	>99
12b	OH		4.5 ± 1.5	1.12 ± .24	127	13	41	98.8

Table 2
Protein kinase activity (IC₅₀ in μM) of key analogs

Compound	AurB	IRAK4	IRAK1	JAK1	JAK2	JAK3	CDK1	CDK2	CDK9
1	0.275 ± 0.03 ^a	>30	>30	>30	>30	>30	>30	>30	>30
5a	>30	>30	>30	>30	>30	>30	>30	>30	>30
7a	0.0273 ± 0.0004	24.4 ± 2.4	>30	>30	>30	>30	>30	>30	>30
7b	0.689 ± 0.018	>30	>30	>30	>30	>30	>30	>30	>30
7c	0.155 ± 0.011	>30	>30	>30	>30	>30	>30	>30	>30
10	>30	>30	>30	>30	>30	>30	>30	>30	>30
12a	>30	0.579 ± 0.024	>30	>30	>30	>30	>30	>30	>30
14a	5.91 ± 7.12	>30	>30	>30	>30	>30	>30	>30	>30
14b	23.1 ± 2.67	>30	>30	>30	>30	>30	>30	>30	>30
16a	>30	>30	>30	>30	>30	>30	>30	>30	>30
16b	>30	>30	>30	>30	>30	>30	>30	>30	>30
17a	>30	>30	>30	>30	>30	>30	>30	>30	>30
24a	>30	>30	>30	>30	>30	>30	>30	>30	>30
24b	7.51 ± 1.11	>30	>30	>30	>30	>30	>30	>30	>30
24c	>30	>30	>30	>30	>30	>30	>30	>30	>30
27	14.3 ± 0.5	>30	>30	>30	>30	>30	>30	>30	>30
33	>30	>30	>30	>30	>30	>30	>30	>30	>30
37	18.1 ± 0.2	>30	>30	>30	>30	>30	>30	>30	>30

^a N = 2.

was the first prototype prepared (Table 3). This analog retains the conformation of the quinazoline series via an internal hydrogen bond between the amino and keto groups. Additionally, these compounds retain GlmU biochemical activity while increasing selectivity against kinases, as expected (Table 2). Further simplification of the core structure led to the minimum pharmacophore represented by **16a**, and its pyridine analog **14a**. Both compounds are as potent against *H. influenzae* GlmU as the quinazoline series, but are slightly less potent against the *E. coli* enzyme. Interestingly, replacing the methoxy group of **14a** with a nitro group, as in **14b**, slightly improved potency, presumably via an additional H-bond interaction through the nitro group. The crystal structure of **14b**

confirmed that the benzamide core is aligned with the phenyl ring of the quinazoline scaffold (Fig. 2C), and all expected hydrogen bonds were maintained, including the hydrogen bond between the linker nitrogen and Asp 105. Additionally, the position of the terminal aromatic ring was relatively unchanged. Interestingly, the change to the benzamidine core resulted in a dramatic change to the linker portion of the molecule. Most dramatically, the orientation of the terminal amide group flipped, eliminating the hydrogen bond seen between the nitrogen and the backbone carbonyl of Val 223. However, the new position of the amide carbonyl places it within hydrogen bond distance of the backbone amide of Gly 225. In effect, one inhibitor-protein interaction was

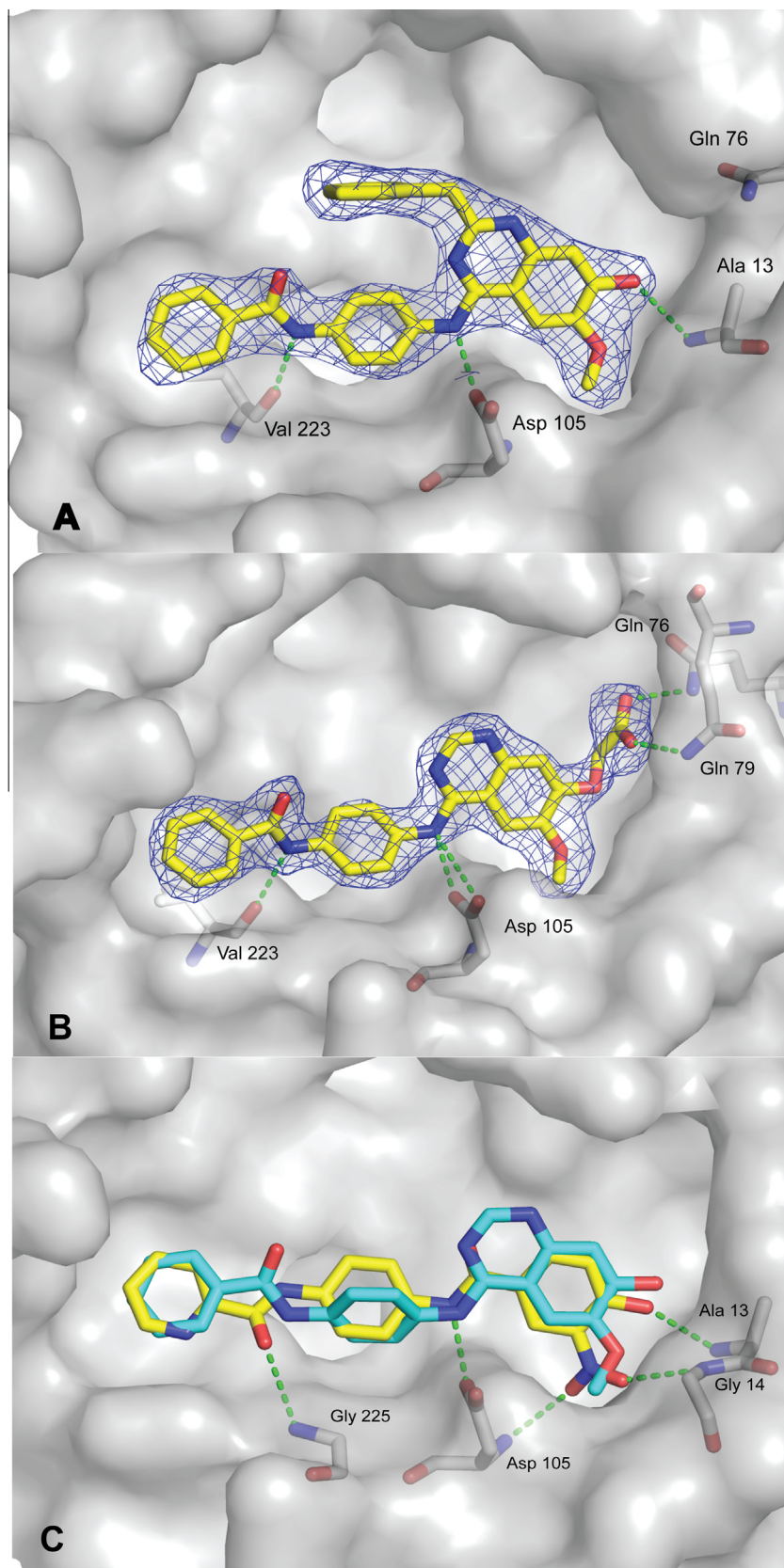
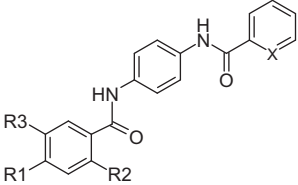
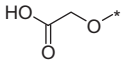
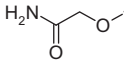


Figure 2. Structures of (A) compound **5c** and (B) compound **7b** in *H. influenzae* GlmU with final $2F_o - F_c$ density (1σ). Hydrogen bonds are shown as dotted lines. (C) Superposition of benzamide compound **14b** (green/light grey) with compound **1** (dark grey). The positions of the benzamide headgroup and the terminal aromatic ring match well with that of the original series. The benzamide headgroup changes the preferred orientation of the linker portion of the molecule.

Table 3



Compound	R1	R2	R3	X	IC ₅₀ (μM)		Solubility			Serum binding (%)
					<i>E. coli</i>	<i>H. influenzae</i>	pH 3.5	pH 7.0	pH 8.0	
14a	OH	H	OMe	N	8.2 ± 3.3	0.51 ± 0.29	10	8.3	23	98.4
14b	OH	H	NO ₂	N	3.1 ± 0.1	0.05 ± 0.007	0.7	18	43	>99
16a	OH	H	OMe	C	18 ± 3.3	1.4 ± 0.2	8.9	8.5	19	>99
16b	OH	NH ₂	OMe	C	5.9 ± 1.1	6.1 ± 0.3	54	18	44	98.9
17a		H	OMe	C	>67	23 ± 3.0	—	—	—	—
17b		H	OMe	C	>22	>22	—	—	—	—

substituted with another resulting in no gain or loss in activity. Finally, attempts were made to extend the benzamide scaffold towards the uracil pocket (compounds **17a** and **17b**), as previously done with the quinazoline scaffold; unfortunately, this effort did not lead to any breakthroughs in potency.

2.2. Fragment identification and characterization

In order to address the moderate potency of the compounds, a virtual screening approach was initiated in order to obtain novel chemical matter as starting points for a new chemical series. Structure-based docking and ligand-based pharmacophore screening utilized both the UTP and GlcNAc substrates as well as known active compounds in order to expand the number of potential hits. Additional areas of the binding site not engaged in inhibitor interactions were also targeted. Fragments were selected for this virtual screen in order to increase diversity of the potential hits. After visual inspection of the highest scoring hits in the virtual screen, 320 fragments were selected for single point inhibition testing in the *H. influenzae* GlmU assay. Active compounds (>33% activity at 10 mM concentration) were further characterized through dose response and nephelometry experiments. An additional compound quality check was performed by liquid chromatography/mass spectrometry. Two fragments, compound **38** and **39**, were identified, postulated to bind in the uracil pocket and selected for further structural and biophysical studies (Fig. 3A).

NMR experiments were performed to confirm binding to the UTP pocket. WaterLOGSY experiments with compound **38** and compound **39** indicated that the compounds bound to *H. influenzae* GlmU (data not shown). Subsequent addition of UTP resulted in intensity reduction of both compounds' WaterLOGSY signals, which is indicative of competitive binding of the fragments with UTP (data not shown). While a complex of compound **38** with *H. influenzae* GlmU could not be obtained likely due to its poor solubility, the structure of compound **39** was solved to a resolution of 2.1 Å (Fig. 3B). This fragment binds in the uracil binding site as predicted, with a tight network of contacts with Gln76 and the backbones of Ala13 and Gly81. An overlay of the fragment with the benzamide series revealed that the phenyl ring of the fragment overlapped with the hydroxy-methoxy phenyl headgroup of **14b**, suggesting that the uracil moiety could be merged onto the benzamide series (Fig. 3C).

2.3. Structure–activity relationships: Hybrid analogs

The first hybrid prototype prepared, **20**, added the uracil unit of compound **38**, the headgroup with superior ligand efficiency¹⁰ onto the minimum pharmacophore **16a**, resulting in a significant increase in biochemical potency (Table 4). We hypothesized that the hydroxyl group of **20** would no longer contribute to potency, and might even negatively affect the orientation of the uracil unit. Therefore, we further optimized the series by removing this group, and replacing the distal phenyl group with a pyridine. The resulting analog **24a** shows potent inhibitory activity in the nanomolar range against in both *E. coli* and *H. influenzae* GlmU biochemical assays, yet maintains a molecular mass below 500 Da. Although the biochemical potency towards the GlmU protein was dramatically improved, solubility and plasma protein binding were negatively affected.

In order to confirm the binding mode of the new series, the structure of **24a** was solved to 2.25 Å in *H. influenzae* GlmU. The interactions seen with the fragment and the benzamide series were maintained in the hybrid structure (Fig. 3C). Some flexibility is seen in the uracil binding pocket to accommodate the slight difference in the position of the uracil group when attached to the larger molecule.

Analysis of the phenyl ring (Table 4, compounds **24a**, **24b**, and **24c**) yielded potent analogs, and confirmed the negative contribution of the substituent ortho to the uracil group. From this set, the 3-methoxy substitution also emerged as the most favorable, and was used for further investigation of uracil replacements (**30a**, **30b**, **33**, and **36**). Overall, while all uracil replacements showed a fair level of activity, none matched the potency of the uracil analog **24a**. These analogs also share significant challenges associated with solubility and protein binding.

The attempts to restore pharmaceutical properties while maintaining fair levels of biochemical potency are summarized in Table 5. The working hypothesis was that the *N*-benzoyl-1,4-phenylene-diamine unit of the minimum pharmacophore **16a** played a major role in negatively impacting plasma protein binding and aqueous solubility. With potent compounds in hand, modifications were introduced that were predicted to improve solubility. In all cases, the analogs prepared did have a drop in biochemical potency, which appeared more pronounced in *H. influenzae* compared to *E. coli*. Simpler amides containing sp³ hybridized carbons

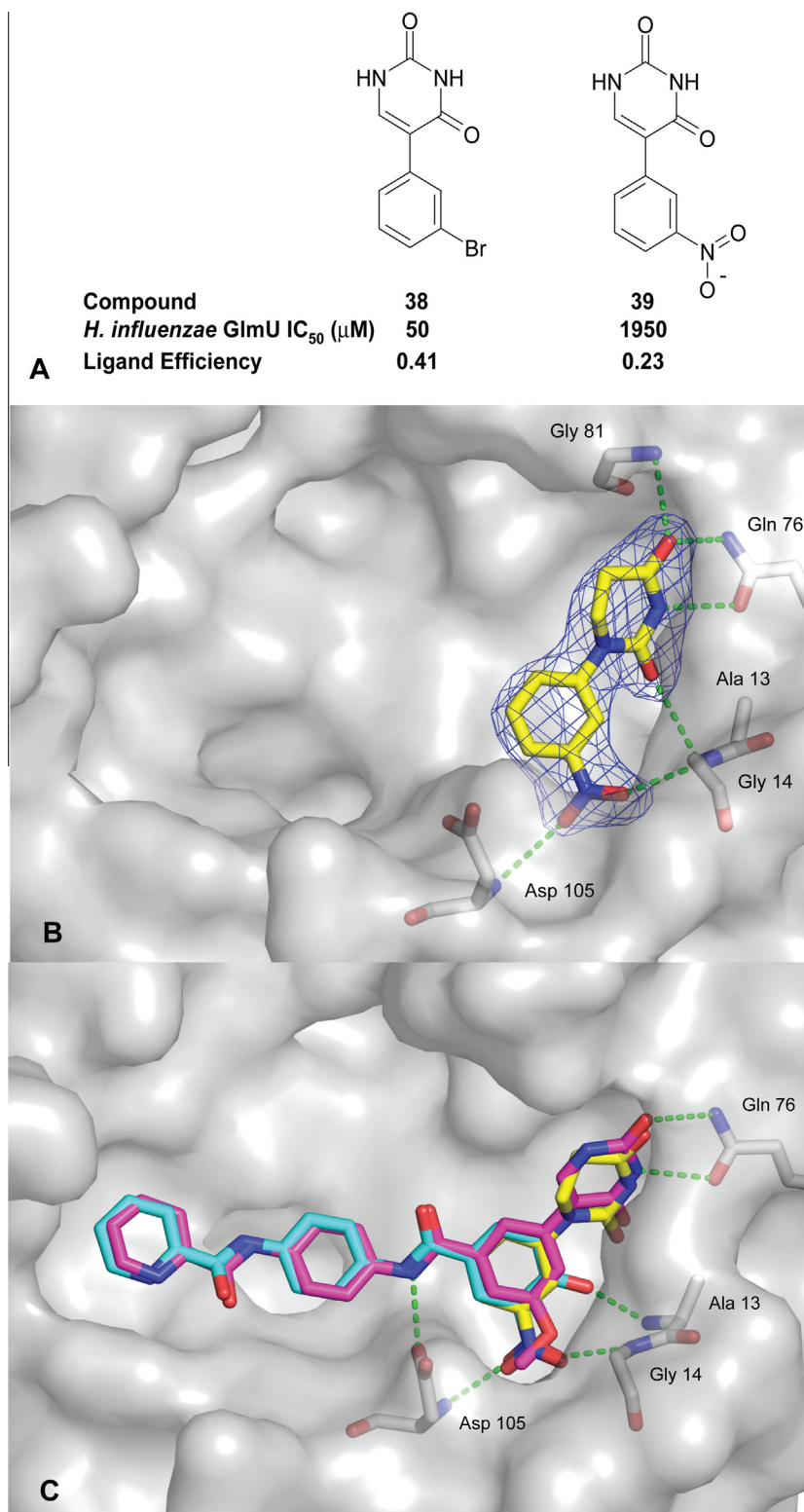
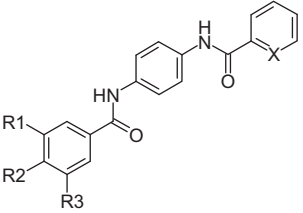


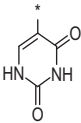
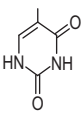
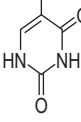
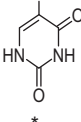
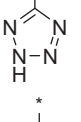
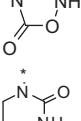
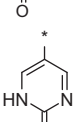

Figure 3. (A) Structures, assay results and ligand efficiencies of fragment compounds found by virtual screening. (B) Structure of compound **39** in *H. influenzae* GlmU with final $2F_o - F_c$ density (1s). Hydrogen bonds are indicated as dotted lines. (C) Superposition of compounds **39** (green) and **14b** (cyan) onto the hybrid compound **24a** (magenta).

such as **27** are well tolerated, yielding balanced activity in both *E. coli* and *H. influenzae* GlmU biochemical assays, and much improved solubility and plasma protein binding. Finally, a simple ethyl urea, as in **37**, also provides a promising avenue for future

investigation. While these analogs only represent a small set of the possible variations, this study clearly demonstrates the significant potential to modulate pharmaceutical properties with this section of the molecule.

Table 4



Compound	R1	R2	R3	X	IC ₅₀ (μM)		Solubility			Serum binding (%)
					<i>E. coli</i>	<i>H. influenzae</i>	pH 3.5	pH 7.0	pH 8.0	
20	OMe	OH		C	0.26 ± 0.03	0.02 ± 0.01	4.7	3.9	8.1	98.1
24a	OMe	H		N	0.027 ± 0.005	0.0017 ± 0.002	0.4	0.3	0.3	-
24b	H	H		N	0.35 ± 0.01	0.005 ± 0.001	2.1	1.6	2.5	98.1
24c	H	OMe		N	>22	0.95 ± 0.45	6.2	5.2	8.4	>99
30a	OMe	H		N	21 ± 2.2	0.55 ± 0.13	0.06	175	188	96.8
30b	OMe	H		N	>22	1.7 ± 0.3	6.4	2.8	4	98.4
33	OMe	H		N	1.7 ± 0.27	0.071 ± 0.011	4.3	3.1	4.7	90.3
36	OMe	H		N	4.2 ± 1.4	0.98 ± 0.02	7.5	7.1	12	>99

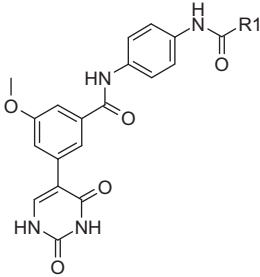
3. Discussion

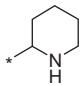
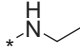
Over the past decade, the discovery of novel antibiotic classes has proven elusive. Previously we reported on a novel class of quinazolines that were specific UTP competitive inhibitors of the bacterial target GlmU uridylyltransferase binding site.⁷ This HTS-based effort had yielded limited SAR, with compounds exhibiting low hundreds of nanomolar activity in in vitro enzyme assays. In this study, we undertook the optimization of this quinazoline lead series in an attempt to improve potency against the target and develop measurable antibacterial activity. This series, exemplified by compound **1**, highlighted the typical challenges often encountered with hits derived from HTS: a relatively flat and lipophilic

molecule, high plasma protein binding, low solubility, modest ligand efficiency and activity against other targets, leading to a selectivity issue.

Since GlmU is an enzyme only found in bacteria, target based selectivity was expected. However, since HTS compounds frequently originate from other drug discovery efforts, off target selectivity is often an issue. Indeed, similar quinazolines to compound **1** have been shown to be potent inhibitors of protein kinases previously,^{11,12} and this series showed similar activities. Potent inhibition such protein kinases would represent a risk of secondary pharmacology that would not be desirable in an antibiotic. Therefore, we decided to first address target potency and selectivity against human protein kinases. Exploitation of X-ray

Table 5



Compound	R1	IC ₅₀ (μM)		Solubility			Serum binding (%)
		<i>E. coli</i>	<i>H. influenzae</i>	pH 3.5	pH 7.0	pH 8.0	
27		0.12 ± 0.04	0.05 ± 0.01	177	160	156	60.5
37		0.097 ± 0.03	0.077 ± 0.01	34	26	67	84.1

crystallography data (both on GlmU and on quinazolines bound to protein kinases) was instrumental in quickly defining rational approaches to manage kinase selectivity. For this effort, we opted to prevent hinge binding either by substitution at the 2-position of the quinazoline ring, or with the elimination of the position one nitrogen atom of the quinazoline via scaffold-hopping (the benzamide series exemplified by **16a**). Both approaches were successful in mitigating the kinase inhibitory activity from the series, while having relatively little effect on GlmU inhibitory activity.

The ability to increase selectivity of the series versus a select set of protein kinases was encouraging. Both approaches taken to mitigate this activity did so by selectively disrupting interactions with the protein kinase and did not directly address the issue of GlmU target potency. Structure-based design of analogs that could enter the GlcNAc pocket was undertaken in an attempt to further drive potency. While the position 2 carbon of the quinazoline scaffold provided an ideal vector to add substituents directed towards and into the GlcNAc pocket, we were unable to establish specific contacts with this region of the enzyme. While potency appeared to be better with some analogs, although not to a level that would not be a step change, neither solubility nor ligand efficiency were improved. Compound size and solubility (ie maximum attainable concentration) are important attributes that affect permeation of Gram-negative outer membranes,¹³ a key requirement to access a cytoplasmic target such as GlmU. The inability to significantly alter these properties while retaining and/or improving potency with our attempts to access the GlcNAc pocket indicated that there was little hope that an inhibitor with antibacterial activity could be identified from this subclass. Alternatively, the ‘deconstruction’ of the quinazoline ring towards benzamides also addressed the kinase selectivity issue, and provided a slightly more favorable minimum pharmacophore **16a** in terms of size, albeit with high plasma protein binding and solubility.

Faced with these challenges, we undertook a virtual screening approach to identify fragment sized compounds that could access binding sites adjacent to that of compounds such as **16a**. In this way we hoped to identify small pharmacophores with good ligand efficiency that could then be exploited in future designs. The virtual screening approach provided two new, small molecule fragments, which could be hybridized with **16a**. The example described here showcases the strength of the fragment screening/hybridization technique in generating new ideas and starting points. The identification of small fragment-like molecules that

could then be incorporated into existing scaffolds using this approach was rapid compared to traditional library synthetic approaches. As was the case for the benzamide series, the ability to exploit X-ray crystallography data and having well characterized binding modes greatly strengthened this approach, increasing its likelihood of success. The resulting hybrid analogs were tight binding (low nanomolar range), representing a breakthrough in potency, and offered a range of new possibilities. Further efforts to improve the physicochemical properties while retaining potency yielded improved compounds (**27** and **37**), but still failed to show significant MICs even in efflux pump deficient strains. Based on these results, it is hypothesized that failure to obtain MICs is not the result of bacterial efflux alone, but rather poor compound flux across the outer membrane. In addition it is likely that further potency gains would be needed, requiring inhibitors with sub-nanomolar activity.

The GlmU binding pocket is very large, and a number of hydrogen bonds are needed to secure the biochemical potencies usually associated with functional activity in bacteria. In addition, subtle SAR differences between the *H. influenzae* and the *E. coli* enzymes were noted, adding further complexity to the identification of broad spectrum Gram-negative compounds targeting this binding site. Nevertheless, the most advanced analogs of the set (**27** and **37**) lose 1–2 logs of potency compared to **24a**, but exhibit balanced activity, with more favorable aqueous solubility and plasma protein binding.

Overall, the design of potent inhibitors of the N-terminal domain of GlmU remains a significant challenge. While we improved potency by 1000 fold in the biochemical assays, functional activity (MICs) remained elusive throughout the program.

4. Material and methods

4.1. GlmU protein expression and purification

E. coli and *H. influenzae* GlmU were expressed and purified as previously described.⁴

4.2. GlmU inhibition assays

Activity (IC₅₀s) of compounds against *E. coli* and *H. influenzae* GlmU was determined using the malachite green based assay similar to that previously described.⁷ The assay mixture consisted of

50 mM Hepes-NaOH buffer (pH 7.5) containing 5 mM DTT, 0.01% Brij-35, 100 μ M EDTA, 0.3 U/mL pyrophosphatase, GlmU isozymes, UTP, and *N*-acetyl-glucosamine-1-phosphate. The concentration of UTP and *N*-acetyl-glucosamine-1-phosphate was 22 and 30 μ M for *H. influenzae*, and 46 and 30 μ M for *E. coli*, respectively. The final concentration of the GlmU isozymes was 0.26 and 0.11 nM for *H. influenzae* and *E. coli*, respectively. Two μ L of a 3-fold serial DMSO dilution of test compound ranging from 10 to 0.041 mM were mixed with 70 μ L of the assay mixture per well in a 96-well plate. After pre-incubation at room temperature for 15 min, 30 μ L of 5 mM $MgCl_2$ were added to initiate the enzyme reaction. The reaction was quenched by addition of 150 μ L of malachite green reagent after 30 min incubation at room temperature, and the absorbance of the solutions was measured at 665 nm using a microplate reader (Envision, PerkinElmer Inc., US). As negative and positive control, DMSO and 20 mM EDTA were used instead of test compounds, respectively. The enzyme inhibitory activity of test compounds was calculated by the following formula: $(O.D._{\text{tested compound}} - O.D._{\text{negative control}}) / (O.D._{\text{positive control}} - O.D._{\text{negative control}})$.

IC_{50} values were calculated by using Kyplot (ver. 5.0, Keyence, Japan). Hill slopes were generally within experimental error of 1 (range 0.7–1.6).

4.3. Kinase selectivity assays

A screening panel of protein kinases with representative members from 4 branches of the kinome was assembled. Activity of Aurora kinase B (AurB), IRAK1, IRAK4, JAK1, JAK2, JAK3, CDK1, CDK2 and CDK9 was determined in vitro using a mobility shift assay on a Caliper LC3000 reader (Caliper, MA), which measures fluorescence of a phosphorylated and unphosphorylated fluorescent peptide substrate and calculates a ratiometric value to determine percent turnover. Phosphorylation of the peptide in the presence and absence of the compound of interest was determined. Enzyme/substrate/adenosine triphosphate (ATP) mix (5 mL) was preincubated with 2 mL of compound for 20 min at 25 °C. Reactions were initiated with 5 mL of 24 mM $MgCl_2$ in 1.2 \times buffer and incubated at 25 °C for 90 min and reactions were stopped by addition of 5 mL of Stop mix consisting of 100 mM HEPES (pH7.3), 121 mM EDTA, 0.8% Coatin Reagent 3 (Caliper, MA), and 0.01% Tween. Phosphorylated and unphosphorylated substrate was detected by a Caliper LC3000 reader (Caliper, MA) in the presence of separation buffer consisting of 100 mM HEPES (pH7.3), 16 mM EDTA, 0.1% Coatin Reagent 3 (Caliper, MA), 0.015% Brij-35, 5% DMSO, and 5.6 mM $MgCl_2$.

4.4. Solubility and plasma protein binding measurements

The solubility of test compounds at three different pH values was measured by a solution-precipitation method as follows. Solutions containing 200 μ M of test compound were prepared by diluting 10 mM compound, dissolved in 100% (v/v) DMSO, into each of three buffer solutions (0.1 M citrate buffer at pH 3.5, 0.1 M phosphate buffer at 7.0, and EPPS (3-[4-(2-hydroxyethyl)-1-piperazinyl]propane-sulfonic acid) buffer at 8.0) directly into a 96-well filter plate device (0.22 μ m pore size filter, MultiScreen HTS, Millipore, US). These solutions were incubated for 90 min shaking at 2000 rpm at 20 °C (M-BR 022UP Taitec Bioshaker, Taitec, Japan). After centrifugation of the filter plate to remove any precipitate, the compound concentration in the filtrate was determined by high performance liquid chromatography (HPLC) analysis. An HPLC system LC20A series (Shimadzu Corporation, Japan), consisting of a model LC20AT pump, a model CTO-20A autosampler, a model CTO-20A column oven, and a model SPD-20A ultraviolet light detector, was used. The HPLC separation was performed using reverse phase C18 column (ODS80-TM, 5 μ m, 4.6 \times 150 mm, Tosoh Bioscience LLC., Japan) at a flow rate of 1 mL/min with 254 nm UV detection. The column temperature was set at 40 °C. The mobile phase was consisted of acetonitrile and water containing 20 mM sodium 1-decansulfonate (Tokyo Chemical Industry, Japan), 40 mM phosphoric acid (Wako Pure Chemical Industries, Japan), and 0.2% (v/v) triethylamine (Wako Pure Chemical Industries, Japan) (40:60 to 50:50, v/v).

Human serum protein binding was determined by an ultrafiltration method using a 96-well filter plate device (10 kDa cut-off membrane filter, MultiScreen PPB, Millipore, US) and human serum (Sigma-Aldrich, US). The protein binding was calculated by following formula: Protein binding (%) = $100 \times (C_t - C_u) / C_t$, where C_u and C_t are the bound-free and total concentrations of test compounds in the serum solution, respectively. For the measurement of C_u , 10 μ M test compound solution was prepared by diluting a 1 mM solution of compound dissolved in 100% (v/v) DMSO with human serum onto the well of the filter plate, and incubated for 30 min at 37 °C. After centrifugation of the filter plate, the compound concentration in the serum filtrate was determined by HPLC analysis. For the measurement of C_t , 10 μ M test compound solution was prepared in 0.05 M phosphate buffer containing 0.09 M sodium chloride (pH 7.4), and analyzed with HPLC.

4.5. Virtual screening methodology

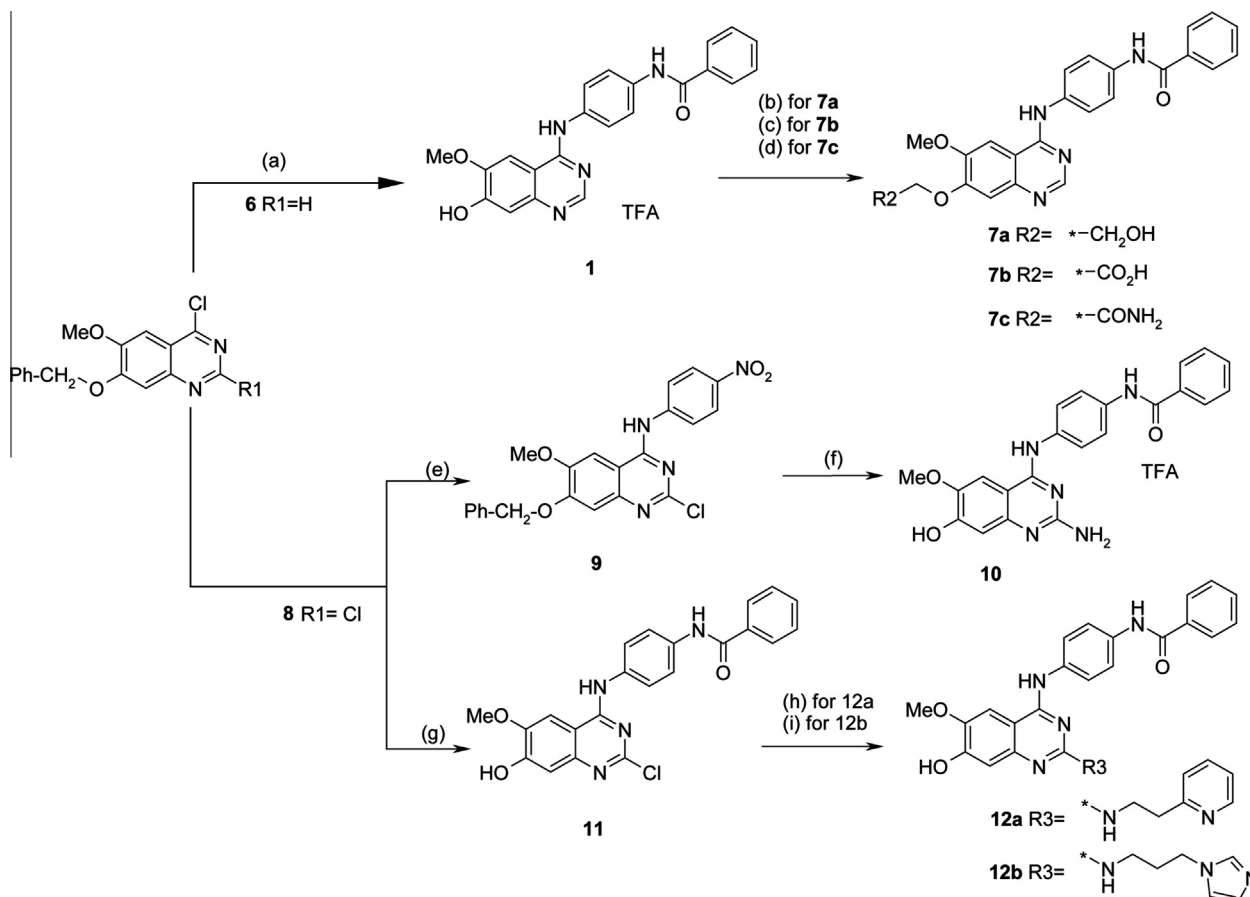
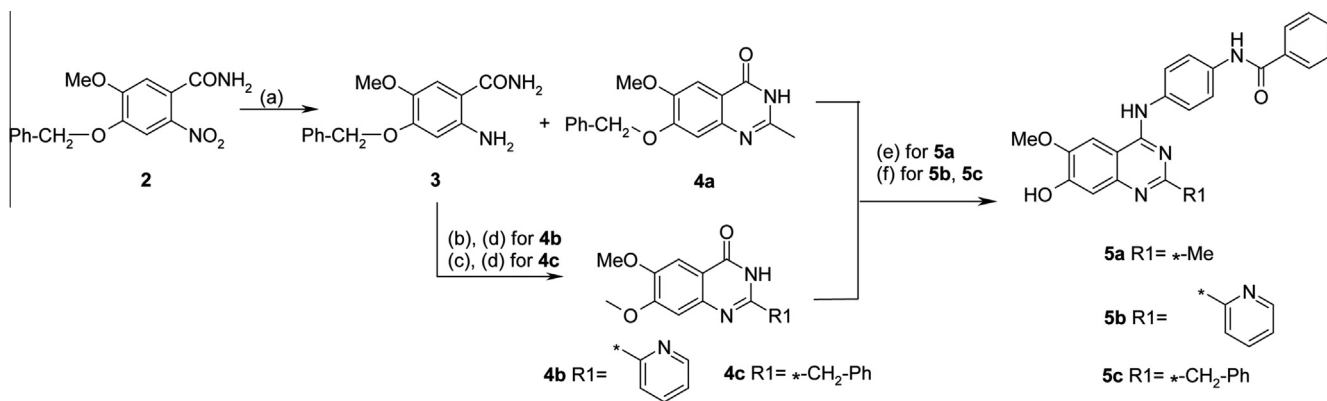
Structure-based virtual screening was performed using a *H. influenzae* GlmU crystal structure. The PPREP module of Maestro

Table 6
Crystallographic data collection and refinement statistics

	5c	7b	14b	39	24a
Space group	H32	H32	H32	H32	H32
Cell constants <i>a</i> ; <i>b</i> ; <i>c</i> (Å)	109.3; 109.3; 328.0	108.7; 108.7; 326.2	108.2; 108.2; 325.9	108.8; 108.8; 327.5	108.2; 108.2; 327.9
Cell constants α ; β ; γ (°)	90; 90; 120	90; 90; 120	90; 90; 120	90; 90; 120	90; 90; 120
Resolution limit (Å)	2.10	1.90	2.21	2.09	2.31
Resolution Range (Å)	42.0–2.10 [2.18–2.10]	40.8–1.90 [1.97–1.90]	31.04–2.21 [2.32–2.21]	48.7–2.09 [2.15–2.09]	30.6–2.31 [2.39–2.31]
Completeness overall (%)	99.9 [100]	99.8 [100]	98.6 [100]	99.5 [96.3]	99.6 [99.6]
Reflections, unique	42262	55796	36717	41865	32767
Multiplicity	6.9 [6.7]	10.0 [9.7]	10.9 [10.5]	7.8 [7.1]	9.9 [4.5]
R_{sym} (%)	11.2 [52.7]	7.6 [52.1]	8.1 [39.8]	7.6 [47.6]	6.5 [37.8]
R -factor _{overall} (%) ²	21.6	20.5	18.5	22.6	19.4
R -factor _{free} (%)	24.9	21.7	22.6	20.0	23.6
Non-hydrogen protein atoms	3442	3442	3437	3426	3442
Non-hydrogen ligand atoms	88	82	86	75	92
Solvent molecules	427	584	615	510	366
PDB accession code	4KNR	4KNX	4KPX	4KPZ	4KQL

(Schrodinger, LLC, Portland, OR) was used for protein preparation at pH = 7. After addition of hydrogens, the protein was subjected to molecular mechanics refinement using the OPLS2001 force field incorporated in IMPREF and minimized until the RMSD reached 0.3 Å.² The minimized structure was used for docking. Water molecules within the active site were removed before generating the

docking grid (Schrodinger, Oregon, USA). The fragment library was assembled using compounds from the internal corporate collection as well as commercially available molecules. 3D conformations were generated using Schrodinger's LigPrep. The fragments were subjected to hydrogen additions, ionization (from pH 5–9) and generation of low-energy ring conformations. The



chiralities of the fragments were preserved. Rigid receptor docking was performed using Schrodinger's Glide software.¹⁴ The docking grid was generated using a box size of $(18 \times 18 \times 18) \text{ \AA}^3$ and the ligand range was defined using an inner box of $(12 \times 12 \times 12) \text{ \AA}^3$. Hits were ranked using Gscore scoring function. Final compounds for enzymatic assay were selected after manual visualization.

4.6. NMR

NMR binding experiments were conducted at 298°K on a 600 MHz NMR instrument with a Bruker AVANCE III console and a triple-resonance cryogenic probe. In the WaterLOGSY experiment,¹⁵ the first water-selective 180° Sinc pulse was 6 ms long, and a weak rectangular pulse field gradient was applied during the mixing time (1.8 s). A gradient recovery time of 2 ms was introduced after the mixing time. Water suppression was achieved by the excitation sculpting scheme¹⁶ and the water-selective 180° Sinc shape pulse was 3 ms long. The data were collected with a sweep width of 9157 Hz, 0.45 s acquisition time and 1.8 s for the relaxation delay. 64 scans were recorded for each experiment, which resulted in 5 min per spectrum. The data were zero filled to 32768 complex points and multiplied by an exponential function (line broadening 3 Hz) prior to Fourier transformation. In a typical WaterLOGSY experiment, 200 μM compound was added to 20 μM *H. influenzae* GlmU in 50 mM HEPES pH 7.5, 5 mM MgCl_2 , 5 mM DTT, 0.1 mM EDTA and 5% D_2O to examine binding; 200 μM UTP was then added to the same sample to compare the change of signal intensities.

4.7. Crystallography

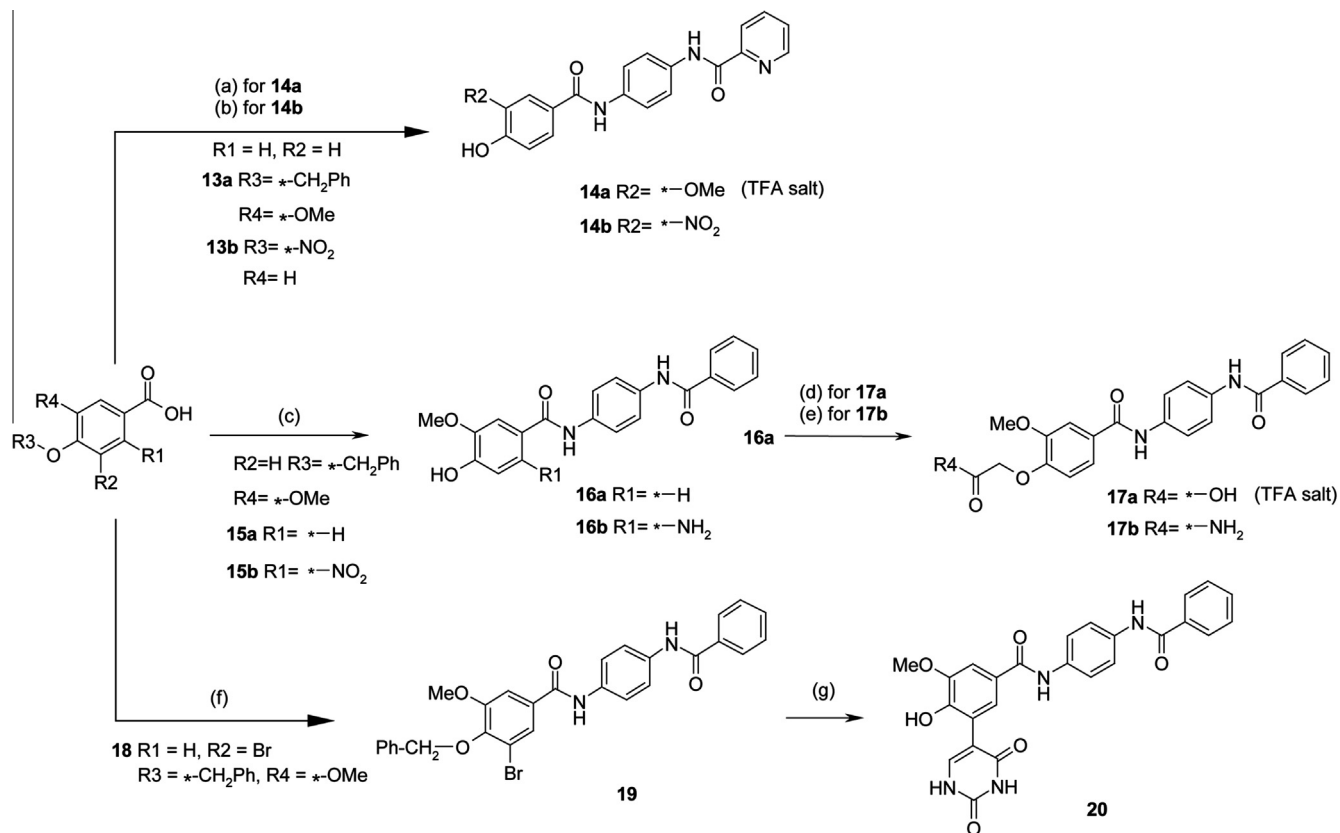
Crystallization and structure determination of complexes with *H. influenzae* GlmU was performed as previously described.⁷ Data were collected on either a Fre+ rotation anode using a Saturn 944+ detector (Rigaku) or at the LRL-CAT beamline at the Advanced Photon Source. Internal structures (data not shown) were used as molecular replacement probes using AmoRe.¹⁷ Refinement was performed using Refmac.¹⁸ with model building and water placement performed using Coot.¹⁹ Final data collection, refinement statistics and PDB accession codes are reported in Table 6.

4.8. Susceptibility testing

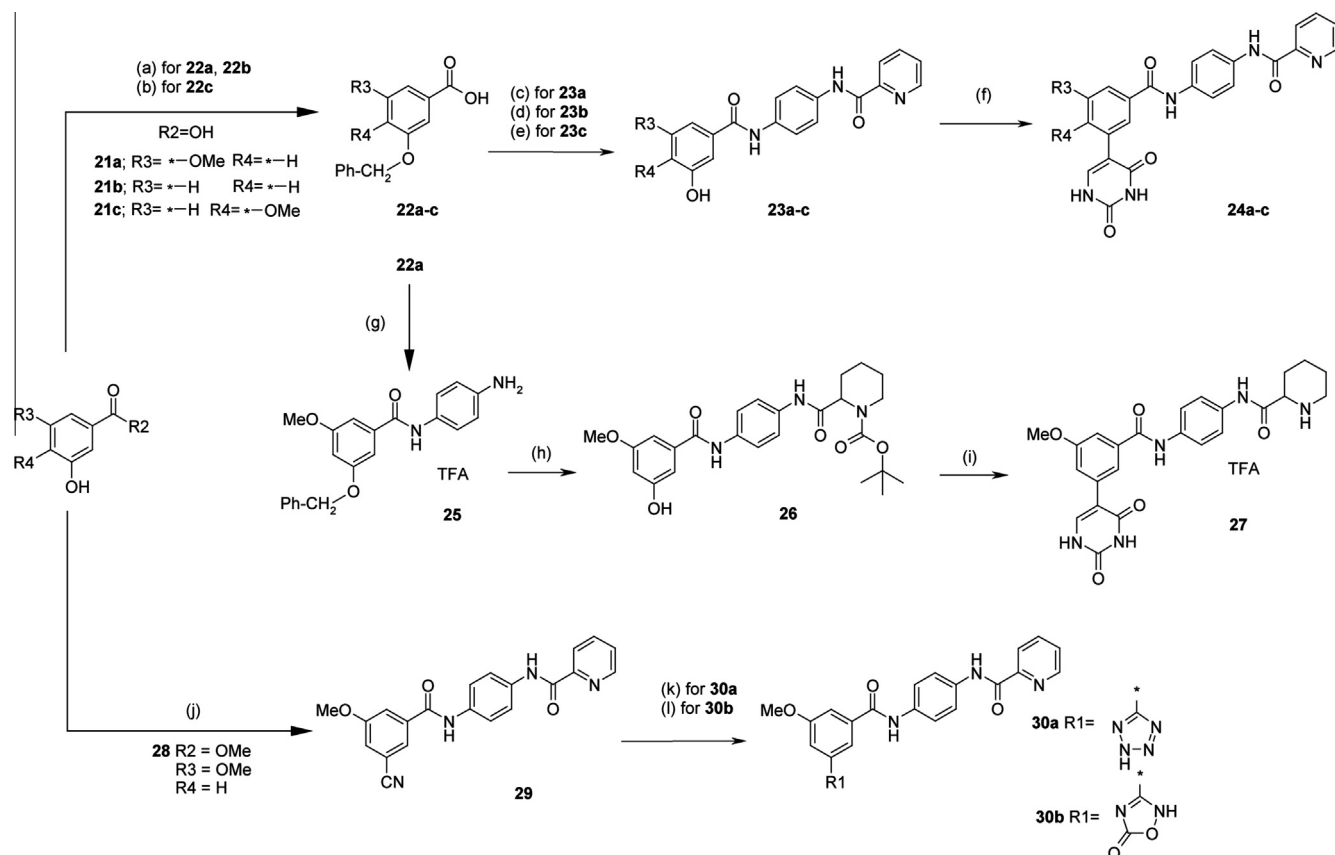
The minimum inhibitory concentration (MIC) was determined by agar dilution method according to standard methods described by the Japanese Society of Chemotherapy.²⁰

One loop of bacteria was incubated in 3 mL Muller Hinton Broth (MHB, Becton Dickinson and Company, US) at 37 °C for 18–24 h, and 100-fold diluted with saline to prepare the 10^6 cfu/mL of inoculating solution of bacteria. For *Streptococcus pneumoniae*, *Streptococcus pyogenes*, *H. influenzae*, and *Moraxella catarrhalis*, one loop of bacteria cultivated on Chocolate II Agar plate (Becton Dickinson and Company, US) was suspended in 3 mL MHB, followed by 25- or 50-fold dilution with MHB to prepare the inoculating solution of the bacteria.

Five μL of bacterial solutions was inoculated onto Muller Hinton Agar (MHA, Becton Dickinson and Company, USA) plates



Scheme 3. Reagents and conditions: (a) (1) *N*-(4-Aminophenyl)pyridine-2-carboxamide, HBTU, HOBT·H₂O, DIEA, DMF, (2) TFA, anisole; (b) *N*-(4-aminophenyl)pyridine-2-carboxamide, HATU, HOAt, DIEA, DMF; (c) (1) 4'-aminobenzanilide, HBTU, HOBT·H₂O, DIEA, DMF, (2) H₂, Pd(OH)₂/C, EtOH; (d) (1) *tert*-butyl bromoacetate, K₂CO₃, DMF, (2) TFA, CH₂Cl₂; (e) 2-bromoacetamide, K₂CO₃, DMF; (f) 4'-aminobenzanilide, HBTU, HOBT·H₂O, DIEA, DMF; (g) (1) uracil-5-boronic acid, Pd(dppf)₂Cl₂, 2 mol/L Na₂CO₃ aq, DMF, (2) TFA.



Scheme 4. Reagents and conditions: (a) (1) benzylbromide, K₂CO₃, DMF, (2) 1 mol/L NaOH aq, EtOH; (b) (1) benzylbromide, K₂CO₃, DMF, (2) 1 mol/L NaOH aq, MeOH; (c) (1) *N*-(4-aminophenyl)pyridine-2-carboxamide, HATU, HOAt, DIEA, DMF, (2) H₂, Pd(OH)₂/C, EtOH; (d) (1) *N*-(4-aminophenyl)pyridine-2-carboxamide, HBTU, HOBT-H₂O, DIEA, DMF, (2) H₂, Pd/C, MeOH, DMF; (e) (1) *N*-(4-aminophenyl)pyridine-2-carboxamide, HATU, HOAt, DIEA, DMF, (2) H₂, Pd/C, DMF; (f) (1) PhNTf₂, K₂CO₃, THF, (2) uracil-5-boronic acid, Pd(dppf)₂Cl₂, 2 mol/L Na₂CO₃ aq, DMF; (g) (1) *N*-Boc-*p*-phenylenediamine, HBTU, HOBT-H₂O, DIEA, DMF, (2) TFA, CH₂Cl₂; (h) (1) Boc-*L*-pipecolic acid, HBTU, HOBT-H₂O, DIEA, DMF, (2) H₂, Pd/C, MeOH, DMF; (i) (1) PhNTf₂, K₂CO₃, THF, (2) uracil-5-boronic acid, Pd(dppf)₂Cl₂, 2 mol/L Na₂CO₃ aq, DMF, (3) TFA, CH₂Cl₂; (j) (1) Tf₂O, pyridine, CH₂Cl₂, (2) ZnCN₂, Pd(Ph₃P)₄, DMF, (3) LiOH-H₂O, water, THF, (4) *N*-(4-aminophenyl)pyridine-2-carboxamide, HBTU, HOBT-H₂O, DIEA, DMF; (k) NaN₃, Et₃N-HCl, toluene; (l) (1) K₂CO₃, NH₂OH-HCl, DMF, (2) CDI, THF.

containing serial 2-fold dilutions of each test compound ranging from 128 to 0.002 µg/mL. MHA supplemented with Sheep defibrinated whole blood (5%, v/v, Nippon Bio-Supply Center, Japan) and MHA supplemented with Fildes extract (5%, v/v, Oxoid Ltd, UK) were used instead of MHA for *S. pneumoniae* and *S. pyogenes*, and *H. influenzae* and *M. catarrhalis*, respectively. After incubation at 37 °C for 18–24 h, the MIC was determined as the lowest compound concentration, at which bacterial growth is invisible.

4.9. Chemical synthesis

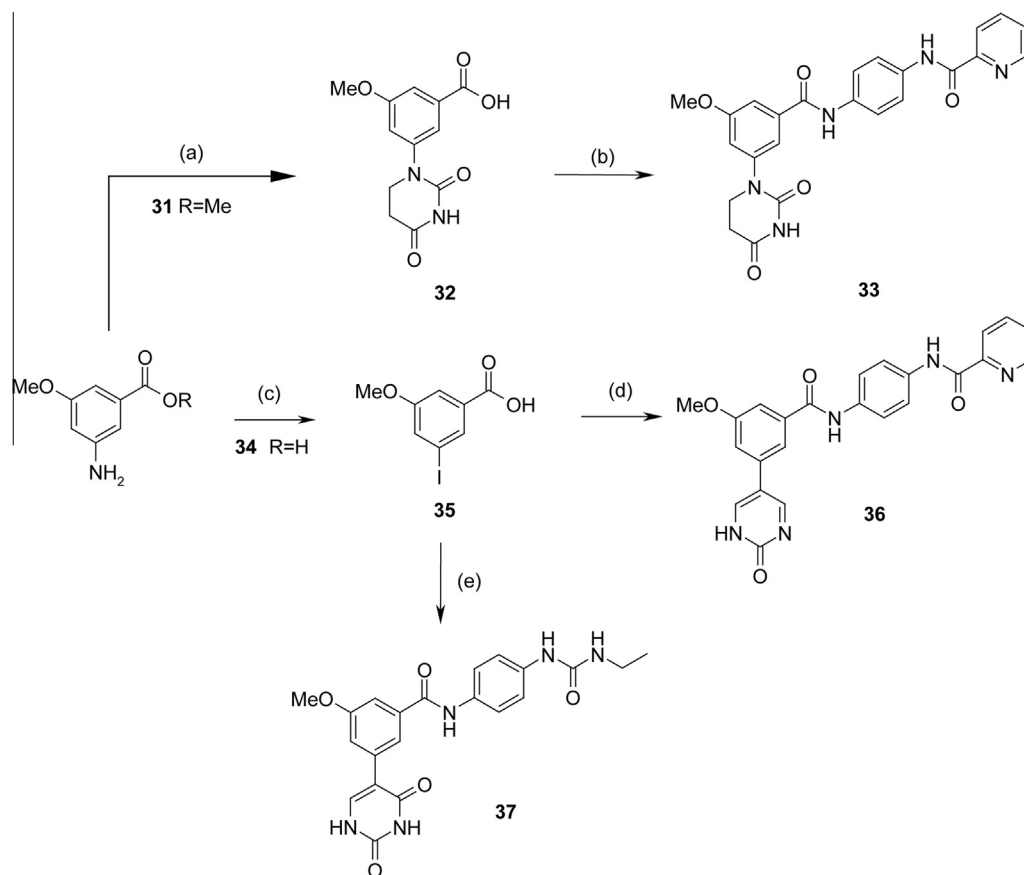
Detailed synthetic routes for the quinazoline and benzamide derivatives prepared in this work are summarized in the Scheme 1–5 and in [Supplementary materials](#). For the quinazoline series, starting materials such as 4-benzyloxy-5-methoxy-2-nitrobenzamide **2**,²¹ 7-benzyloxy-4-chloro-6-methoxyquinazoline **6**²² and 7-benzyloxy-2,4-dichloro-6-methoxyquinazoline **8**²¹ were prepared according to previously described methods.

Compound **3** was obtained by reduction of the nitro group of **2**, leaving the 2-methyl quinazoline **4a** as a side product. Compounds **4b** and **4c** were prepared by reaction of **3** with appropriate acid chlorides followed by alkaline treatment. Preparations of C-substituted quinazolines **5a–c** were completed by chlorination with phosphorus oxychloride and reaction with 4'-aminobenzanilide followed by treatment with trifluoroacetic acid ([Scheme 1](#)). Our lead compound **1** ([Scheme 2](#)) was prepared by reaction of **6** with 4'-amino-

benzanilide under acidic conditions followed by debenzylation. A small series of O-alkylations with appropriate halides led to quinazoline derivatives **7a–c**. Preparation of 2-aminoquinazoline **10** was achieved by reaction of **8** with 4-nitroaniline, reaction with 2,4-dimethoxybenzylamine under microwave irradiation, nitro group reduction and acylation, followed by deprotection. *N*-substituted **12a** and **12b** were obtained by catalytic debenzylation of **8**, leading to **11**, and sequential displacement of the two chlorine atoms with 4'-aminobenzanilide and the appropriate primary amines.

Benzamides **14a** and **14b** can be prepared ([Scheme 3](#)) from corresponding carboxylic acids **13a** and **13b** via amide bond forming reaction with *N*-(4-aminophenyl)pyridine-2-carboxamide and deprotection as needed. Benzamides **16a** and **16b** were obtained from corresponding carboxylic acids **15a** and **15b** via amide bond forming reaction with 4'-aminobenzanilide followed by catalytic hydrogenation. Further O-alkylation of compound **16a** afforded the substituted acetate **17a** and acetamide **17b**. Lastly, uracil-substituted benzamide **20** can be accessed from the brominated carboxylic acid **18** via amide bond forming and Suzuki coupling with uracil boronic acid, followed by deprotection.

The preparation of uracil-substituted benzamides **24a–c** ([Scheme 4](#)) from the corresponding carboxylic acids **21a–c** involved an amide bond forming reaction with *N*-(4-aminophenyl)pyridine-2-carboxamide as a key step. The Suzuki coupling with uracil boronic acid was enabled by activations via triflate. Several



Scheme 5. Reagents and conditions: (a) (1) acrylic acid, toluene, (2) urea, AcOH; (3) 1 mol/L NaOH, MeOH; (b) *N*-(4-aminophenyl)pyridine-2-carboxamide, HATU, HOAt, DIEA, DMF; (c) (1) NaNO₂, concd HCl, water, (2) KI, water; (d) (1) *N*-(4-aminophenyl)pyridine-2-carboxamide, HATU, HOAt, DIEA, DMF, (2) 2-chloropyrimidine-5-boronic acid, Pd(dppf)₂Cl₂, 2 mol/L Na₂CO₃ aq, DMF; (3) AcONa, AcOH; (e) (1) *N*-Boc-*p*-phenylenediamine, HBTU, HOBT-H₂O, DIEA, DMF, (2) TFA, CH₂Cl₂, (3) phenyl chloroformate, pyridine, CH₂Cl₂, (4) EtNH₂, Et₃N, DMF, (5) uracil-5-boronic acid, Pd(dppf)₂Cl₂, 2 mol/L Na₂CO₃ aq, DMF.

protection/deprotection sequences were necessary to complete these routes. Piperidine **27** followed a similar scheme, this time from carboxylic acid **22a** according to the similar procedure of preparations of **24a–c**. Lastly, the cyano-benzamide intermediate **29** allowed the preparation of tetrazole **30a** and oxadiazolidinone **30b** according to conventional methods.

Preparation of **33** (Scheme 5) was achieved via reaction of aniline **31** with acrylic acid and cyclization with urea, followed by amide bond forming reaction with *N*-(4-aminophenyl) pyridine-2-carboxamide. Standard conversion of a similar starting material to iodide **35** followed by sequential amide bond formation and Suzuki couplings, according to the similar procedure of preparations of **24a–c**, led to analogs **36** and **37**.

4.10. General

¹H NMR spectra were recorded with a JEOL JNM-ECP500 (500 MHz) or a Varian NMR System PS500 (500 MHz). Chemical Shifts are given in part per million (ppm) using tetramethylsilane as the internal standard for spectra obtained in DMSO-*d*₆ or CDCl₃. All *J* values are given in Hz. Mass (MS) were measured on a Finnigan LTQ mass spectrometer using ESI for ionization. Column chromatography was performed with indicated solvents using Merck silica gel 60 (70–230 mesh) or Biotage KP-SIL (Silica) cartridge (40–63 mm, 60Å). Monitoring of reactions was carried out using Merck 60 F254 silica gel, glass-supported TLC plates, followed by visualization with UV light (254 nm) and staining with iodine

vapor. Reagents and solvents were used as obtained from commercial supplier without further purification.

Acknowledgments

The authors wish to thank Vanitha Subramanian and Allan Wu for their laboratory assistance and Dr. Steve Wasserman and the staff at LRL-CAT for crystallographic data collection.

Supplementary data

Supplementary data associated with this article can be found, in the online version, at <http://dx.doi.org/10.1016/j.bmc.2014.08.017>.

References and notes

- Silver, L. L. *Clin. Microbiol. Rev.* **2011**, *24*, 71.
- Gehring, A. M.; Lees, W. J.; Mindiola, D. J.; Walsh, C. T.; Brown, E. D. *Biochemistry (N.Y.)* **1996**, *35*, 579.
- Milewski, S.; Gabriel, I.; Olchow, J. *Yeast* **2006**, *23*, 1.
- Buurman, E. T.; Andrews, B.; Gao, N.; Hu, J.; Keating, T. A.; Lahiri, S.; Otterbein, L. R.; Patten, A. D.; Stokes, S. S.; Shapiro, A. B. *J. Biol. Chem.* **2011**, *286*, 40734.
- Pereira, M. P.; Blanchard, J. E.; Murphy, C.; Roderick, S. L.; Brown, E. D. *Antimicrob. Agents Chemother.* **2009**, *53*, 2306.
- Mochalkin, I.; Lightle, S.; Narasimhan, L.; Bornemeier, D.; Melnick, M.; Vanderroest, S.; McDowell, L. *Protein Sci.* **2008**, *17*, 577.
- Larsen, N. A.; Nash, T. J.; Morningstar, M.; Shapiro, A. B.; Joubran, C.; Blackett, C. J.; Patten, A. D.; Boriack-Sjodin, P. A.; Doig, P. *Biochem. J.* **2012**, *446*, 405.
- Caporuscio, F.; Tañi, A. *Curr. Med. Chem.* **2011**, *18*, 2543.

9. Bridges, A. J.; Zhou, H.; Cody, D. R.; Rewcastle, G. W.; McMichael, A.; Showalter, H. D.; Fry, D. W.; Kraker, A. J.; Denny, W. A. *J. Med. Chem.* **1996**, 39, 267.
10. Abad-Zapatero, C. *Expert Opin. Drug Discov.* **2007**, 2, 469.
11. Marzaro, G.; Guiotto, A.; Chilin, A. *Exp. Opin. Ther. Patents* **2012**, 22, 223.
12. Mortlock, A. A.; Keen, N. J.; Jung, F. H.; Heron, N. M.; Foote, K. M.; Wilkinson, R. W.; Green, S. *Curr. Top. Med. Chem.* **2005**, 5, 807.
13. Pages, J. M.; James, C. E.; Winterhalter, M. *Nat. Rev. Microbiol.* **2008**, 6, 893.
14. Friesner, R. A.; Banks, J. L.; Murphy, R. B.; Halgren, T. A.; Klicic, J. J.; Mainz, D. T.; Repasky, M. P.; Knoll, E. H.; Shelley, M.; Perry, J. K.; Shaw, D. E.; Francis, P.; Shenkin, P. S. *J. Med. Chem.* **2004**, 47, 1739.
15. Dalvit, C.; Fogliatto, G.; Stewart, A.; Veronesi, M.; Stockman, B. *J. Biomol. NMR* **2001**, 21, 349.
16. Stott, K.; Stonehouse, J.; Keeler, J.; Hwang, T.; Shaka, A. J. *J. Am. Chem. Soc.* **1995**, 117, 4199.
17. Bailey, S. *Acta Cryst.* **1994**, D50, 760.
18. Murshudov, G. N.; Vagin, A. A.; Dodson, E. J. *Acta Crystallogr. Sect. D: Biol. Crystallogr.* **1997**, 53, 240.
19. Emsley, P.; Lohkamp, B.; Scott, W. G.; Cowtan, K. *Acta Cryst.* **2010**, D66, 486.
20. Japan Society of Chemotherapy *Chemotherapy* **1990**, 38, 102–105.
21. Mortlock, A.; Keen, N.; Jung, F.; Brewster, A. Patent publication number WO 2001021596, 2001.
22. Althuis, T. H.; Hess, H. *J. Med. Chem.* **1977**, 20, 146.
23. Mochalkin, I.; Lightle, S.; Zhu, Y.; Ohren, J. F.; Spessard, C.; Chirgadze, N. Y.; Banotai, C.; Melnick, M.; McDowell, L. *Protein Sci.* **2007**, 16, 2657.